IN-SITU NEUTRON DIFFRACTION CHARACTERIZATION OF TEMPERATURE DEPENDENCE DEFORMATION IN α-URANIUM

C.A. Calhoun[a], E. Garlea[b,*], T. A. Sisneros[c], S.R. Agnew[a]

[a] *Materials Science and Engineering Department, University of Virginia*
[b] *Development Department, Y-12 National Security Complex*
[c] *P-25, Subatomic Physics Department, Los Alamos National Laboratory*

**Corresponding author: garleae@y12.doe.gov*

ABSTRACT

In-situ strain neutron diffraction measurements were conducted at temperature on specimens coming from a clock-rolled α-uranium plate, and Elasto-Plastic Self-Consistent (EPSC) modeling was employed to interpret the findings. The modeling revealed that the active slip systems exhibit a thermally activated response, while deformation twinning remains athermal over the temperature ranges explored (25-150 °C). The modeling also allowed assessment of the effects of thermal residual stresses on the mechanical response during compression. These results are consistent with those from a prior study of room-temperature deformation, indicating that the thermal residual stresses strongly influence the internal strain evolution of grain families, as monitored with neutron diffraction, even though accounting for these residual stresses has little effect on the macroscopic flow curve, except in the elasto-plastic transition.

Keywords: uranium, neutron diffraction, residual strain, internal strain, EPSC, Elasto-Plastic Self-Consistent modeling, twinning, deformation modes

1. INTRODUCTION

Orthorhombic α-uranium exhibits high single crystal anisotropy in its elastic [1], thermal expansion [2,3] and plastic response [4,5], which leads to highly anisotropic textured polycrystals. In additional to the anisotropy at a given temperature, studies on single crystals have shown these properties possess individual temperature dependencies [1,3,6]. The single crystal anisotropy is so strong it drives thermal ratcheting in textured materials [7].

The plastic anisotropy is due to the crystallography of the active deformation mechanisms, which include 4 dislocation slip modes and 3 deformation twinning modes [4,5,8]. The four slip modes are, in ascending order of relative strength at room temperature: (1) $[100](010)$, denoted *wall slip*; (2) $[100](001)$, denoted *floor slip*; (3) $^1/_2\langle 1\bar{1}0\rangle\{110\}$, denoted *chimney slip*; and finally, (4) $^1/_2\langle 1\bar{1}2\rangle\{021\}$, denoted *roof slip* [4,5]. Single crystal studies have revealed that, although each of the slip modes have a unique temperature dependence, all of them exhibit a typical thermally activated nature with distinct athermal plateau temperature and stress [6]. Three twinning modes occur, in addition to the slip modes. The $\langle 3\bar{1}0\rangle\{\bar{1}30\}$ twin mode has two twin variants. It is the most widely observed twinning mode and is a compound twin with a shear of 0.299 [4,8,9]. Single crystal studies have shown that this twin mode softens slightly with temperature [6]. The $\langle 3\bar{1}2\rangle\{172\}$ twinning mode has four twin variants and is a type II twin with a shear of 0.227 [4,8,10]. The $\langle 3\bar{7}2\rangle\{112\}$ has four twin variants and is a type I twin with a shear of 0.227. To date, crystal plasticity modeling studies carried out on uranium have neglected this mode since its contribution cannot be discriminated from the $\langle 3\bar{1}2\rangle\{172\}$ and it is seen in smaller fractions [4,8,9].

The anisotropy in the single crystal thermal expansion coefficients leads to the development of thermal stresses during cooling from thermo-mechanical processing temperatures [11]. In the *b* direction, the coefficient of thermal expansion is negative or near zero, while both the *a* and *c* direction exhibit positive thermal expansion [2,3]. These stresses have been shown to induce plastic relaxation mechanisms [11] and even annealed polycrystals exhibit inter-granular residual stresses at room temperature. More actively studied zirconium and its alloys also develop such thermal residual stresses, but the stresses are not high enough to exceed the elastic limit [12].

The Elasto-Plastic Self-Consistent (EPSC) model used to address thermal residual stresses in Zr alloys was extended to approximate residual stresses in α-uranium by allowing plastic relaxation during cooling [11].

While many excellent studies were conducted in the 1950s and 1960s, there have been a few recent studies on the deformation of textured, polycrystalline α-uranium. Brown et al. studied the deformation of clock-rolled plate using in-situ neutron diffraction [13]. Tensile loading experiments along the rolling direction at room temperature, 200 °C, and 400 °C as well as the transverse (in-plane) direction at room temperature showed that the material primarily deformed by slip, as evidenced by the fact that minimal texture evolution occurred (i.e., no large shifts in diffraction peak intensity were observed) until very large strains were developed. The observed decrease in strength with increase in temperature is consistent with slip-based deformation in metals. McCabe et al. studied room temperature deformation behavior using a combination of microstructure characterization using electron backscattered diffraction (EBSD) and conventional stress-strain curve measurement [8]. The Visco-Plastic Self-Consistent (VPSC) model was successfully used to describe the shape of the flow curve and the evolution of the twin volume fractions observed using EBSD. The VPSC model neglects thermo-elastic strains, so the possible effects of the thermal residual stresses were not explored. In a follow up work by Knezevic and co-authors, a VPSC model accounted for the rate and temperature sensitivity of the deformation modes in clock-rolled α-uranium [14]. This study included stress-strain curves collected at various temperatures, primarily in compression along the transverse and through-thickness directions. The model well described tests performed under quasi-static and dynamic (Kolsky bar) testing conditions at various temperatures.

The same authors previously analyzed the effects of thermal residual stresses on room temperature deformation using an EPSC model and in-situ strain neutron diffraction [15]. Samples cut from an annealed plate were subjected to uniaxial compression loading along the rolling and transverse directions in a clock rolled plate as well tension along the rolling direction. It was confirmed that twinning serves as a dominant deformation mechanism during compression along the rolling direction at room temperature.

In this paper, the in-situ neutron diffraction results and EPSC modeling reported previously are extended to investigate the effects of temperature on compressive loading along the rolling

direction in clock-rolled plate. The objective of the work is to determine the extent to which inter-granular thermal residual stresses affect the internal strain evolution.

2. METHODS

2.1.Experimental Methods

The material used for this study is the same as that described in Ref. [13]. The depleted uranium was initially cast as a 254 mm thick ingot, hot cross-rolled at 640 °C to 32 mm, warm clock-rolled* at 330 °C to 15 mm, and then annealed at 480 °C for 2 h. Subsequently, the plate underwent further warm clock-rolling at 330 °C to 7.6 mm and reportedly annealed again at 550 °C for 2h. Samples were electro-discharged machined from the plate, and tested in the as-machined condition with no additional heat treatment. Identical processing conditions were reported by many other researchers [8,13,14]. Despite these nearly identical conditions, significant variations between the responses to loading along the rolling direction (RD) in compression were observed. The grain sizes and textures are very similar across these studies, but the mechanical response varied significantly. Pole figures representing the observed textures in this work were calculated from complete orientation distributions computed using complete diffraction spectra collected on the HIPPO instrument in the Lujan center of Los Alamos National Laboratory (**Figure 1**). More details of the texture measurement can be found in reference [16].

* Clock rolling means the sample was rolled, rotated a prescribed amount (e.g., 45° clockwise) about the plate normal direction, and rolled again, through a series of rolling passes. The net effect is to render the material more isotropic within the plane of the plate/sheet.

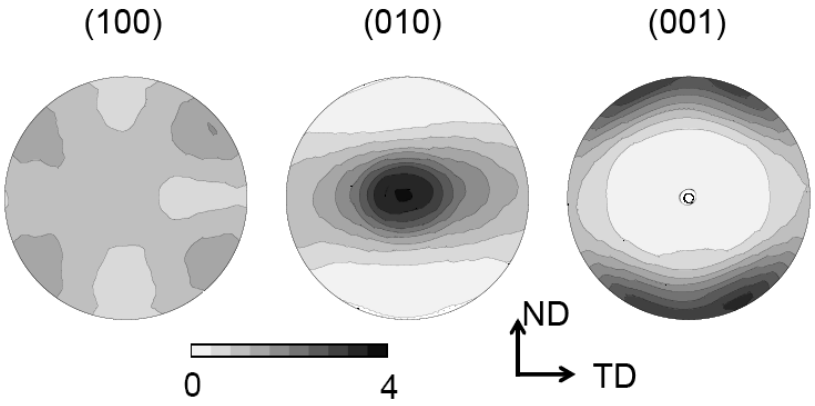

Figure 1. The measured pole figures from the room temperature sample prior to deformation. The loading direction is out of the page parallel to the rolling direction. TD is the transverse direction and ND is the normal direction.

In-situ strain neutron diffraction experiments were conducted at the Lujan User Facility within the Los Alamos Neutron Science Center (LANSCE), on the SMARTS instrument, which is fully described in the literature [13,17]. Shifts in the lattice spacings during deformation of polycrystal samples reveal lattice strains, which are a direct result of either thermal expansion or elastic deformation. Specimens were subjected to compressive loading at room temperature (23 °C), 100 °C, and 150 °C while inside the neutron beam. In-situ heating was performed using a RF furnace, which allowed the sample to remain in the neutron beam throughout the experiment. Samples were loaded incrementally and held long enough to collect sufficient diffraction data (20 minutes per measurement). In the elastic region, this loading is performed in stress increments, but through the elasto-plastic transition and beyond, the loading was done in displacement increments. It is noted that the hold at constant sample displacement results in load relaxation during the dwells, as evidenced by the saw tooth nature of the stress-strain curves (**Figure 2**).

LANSCE is home to a spallation neutron source, which supplies packets of neutrons with a range of velocities (i.e. wave-lengths) to the instruments within the Lujan neutron scattering facility. Knowing the distance between the chopper (time zero location) and the detector, along with the corresponding time of flight, allows for the measurement of the speed, which is then turned into a wavelength via the de Broglie equation: $\lambda = {ht}/{mL}$, where h is Plank's constant, t is the time of flight, m is the mass of an electron, and L is the length of the flight path. From the

wavelength, Braggs' law reveals the lattice- or d-spacing. This allows for fixed diffraction geometry (in contrast with typical x-ray measurements or monochromatic sources of neutrons, where the diffraction angle, 2θ, is varied during an experiment). The position of the ±90° detector banks puts the diffraction vectors in two orthogonal directions, often parallel and perpendicular to the loading direction in the case of uniaxial deformation experiments, as illustrated in previous publications [13,15]. The detectors are located ~ 1.5 m from the sample and are about 0.7 m in width. Given the detector center positions +/- 90°, they subtend $\pm 13°$ about these center positions in 2θ. The detectors are ~ 0.8 m tall and subtend $\pm 15°$ above and below the 2θ plane.

Monitoring the change in lattice spacing for different *hkl* diffraction peaks as a function of macroscopically applied stresses and strains provides insight into the plastic deformation mechanisms. A strain is associated with each *hkl* diffraction peak and is computed using a standard engineering strain definition:

$$\varepsilon^{hkl} = \frac{d^{hkl} - d_o^{hkl}}{d_o^{hkl}} \quad (1)$$

where d^{hkl} is the lattice spacing at the current load increment, and d_o^{hkl} is the lattice spacing at zero macroscopic stress. Ideally, d_o^{hkl} would be the stress-free lattice parameter, but since this material has strong inter-granular (type II) residual stresses and the experimental setup is most accurate at measuring a relative change in lattice spacing, we use the initial value to provide a relative change. The same protocol is employed in the simulation tool described below, such that the comparison between model and experiment is consistent.

It is noted that each *hkl* diffraction peak provides information relevant to all the grains with {*hkl*} planes perpendicular to the diffraction vector. As such, a set of grains denoted {*hkl*} refers to all the grains with an {*hkl*} plane perpendicular to the loading direction. Grains showing higher internal strain often represent hard grains, which resist plastic deformation, since the stress is directly related to the strain (through Hooke's Law). However, elastic anisotropy and thermal residual stresses complicate the direct interpretation of this data, so polycrystalline modeling is required for even an initial assessment. Elastic anisotropy influences the resulting strains, because more compliant grains will exhibit more strain at a given stress. Thermal residual stresses and variations in specimen positioning can affect the d_o^{hkl} value and, thus, the internal strains reported here. As such, it is important to remember that the shifts in lattice strain are actually *relative* shifts

in the elastic strain in grains constrained within a polycrystal, rather than absolute internal strain values relative to stress-free crystals in isolation (i.e., a powder).

2.2. Modeling Approach

The EPSC modeling scheme originally presented in Turner and Tomé [12] is employed. To account for the interaction between grains, each grain is modeled as an ellipsoid inside a homogeneous effective medium, which represents the average response of the polycrystal (i.e. the bulk response). Using the Eshelby solution, the local stresses and strains are computed from the imposed stress and strain state. The effective properties of the aggregate are iteratively converged upon through the self-consistent scheme. The polycrystal is idealized as a collection of ellipsoidal, single crystal grains with unique crystallographic orientations and volume fractions selected to reflect the overall texture. Each grain's response is given by an elasto-plastic single crystal constitutive law, which accounts for the potential activity of the aforementioned slip and twinning modes.

For each slip and twinning system, the resolved shear stress (RSS) is computed, and when it reaches the threshold value, the critical resolved shear stress (CRSS), the possibility of plastic deformation is explored. In order to be activated, the RSS must remain equal to the evolving CRSS throughout the straining increment. In the present study, the RSS values of each of the slip and twinning systems are assumed to evolve in proportion to shear strain accommodated. The model of Clausen et al. is employed to simulate twinning [18]. In this model, a new “child” grain ellipsoid with the correct crystallographic orientation is created each instance that a twin variant is activated for the first time. The volume fraction increment, δv_f, transferred from the parent grain to the child in proportion to the amount of shear, $\delta\gamma_{tw}$, that the twinning variant has accommodated: $\delta v_f = \delta\gamma_{tw}/s_0$, where the proportionality constant s_0 is the characteristic twinning shear. Two key short comings of this model are: (1) only the stress state within the parent grain are considered, i.e. stresses inside the child do not influence further twin propagation [19] and (2) the stress state of the parent (matrix) and child (twin) are not directly coupled. The only explicit coupling between the parent and child is through the volume transfer described above.

Previously, this modeling approach was utilized to predict the development of thermal residual stresses [11], and to analyze the effects of these residual stresses in α-uranium on deformation at room temperature [15]. Here, the thermal residual stress state is computed using a

certain set of CRSS values for cooling (see ref [11]) from 550 °C to room temperature. In order to predict the evolution of thermal residual stresses present within the sample at the beginning of the elevated temperature in-situ compression tests, another set of CRSS values appropriate for lower temperature deformation (25-150 °C) was employed to simulate the stress-free heating prior to simulating the mechanical deformation which is shown in Table 1.

The slip mechanisms are assumed to be thermally activated, while the twinning modes were considered athermal, and the results will be shown to support this assumption. To account for thermal activation of glide, the functional form presented by Knezevic et al. [14] is employed and written as:

$$\tau_\alpha(T) = \tau_{ref} \exp\left(\frac{T - T_{ref}}{B_\alpha}\right) \tag{2}$$

where τ_α is the CRSS at a given temperature, T; $\tau_{ref}$is the CRSS at the reference temperature, T_{ref}, and B_α is a fitting parameter. In the current study, the values of T_{ref} and B_α are the same as those employed by Knezevic et al. The reference CRSS values were based upon a prior study, with slight adjustment to account for lot-to-lot variations, primarily associated with annealing [15]. Values for the rest of the parameters are presented in Table 1.

More sophisticated, state variable (dislocation density) based models have been developed to describe strain hardening behavior, e.g. [14], however the present work is squarely focused on the effect of thermal residual stresses, rather than hardening model development. The shifts in elastic moduli are subtle in comparison with the observed changes in strain hardening rates. Thus, dynamic recovery serves as the primary explanation for differences in the internal strain evolution with temperature. At higher temperature, there is more thermally activated recovery, so the strain hardening rates decrease with temperature.

Table 1. Parameters used in EPSC modeling, the three values of θ for the roof and chimney model correspond to room temperature (RT)/ 100 °C/ 150 °C

Mode	$\boldsymbol{\tau_{ref}}$	$\boldsymbol{B_{\alpha}}$	$\boldsymbol{\theta}$
Wall	15	250	50
Floor	90	230	50
Roof	200	1000	400/220/100
Chimney	150	160	200/110/50
$\{\bar{1}30\}$	90	-	5
$\{\bar{1}72\}$	325	-	150

In practice, the linear hardening rates were calibrated to the room temperature data. Next, using the previously modeled temperature sensitivities of the CRSS values, the hardening rates were adjusted for the two harder modes, roof and chimney, to fit the flow stress data collected at 150 °C. The hardening rates of the two soft (floor and wall) modes were not fitted, because the predicted macroscopic response was insensitive to those values. Instead, the linear hardening rates of the floor and wall modes were scaled in proportion to the decrease in shear modulus, for which Knezevic et al. reported functional forms [14]. The values for the 100 °C case were linearly interpolated between the values fitted to the room temperature and 150 °C data, given the narrow temperature range. A complete list of parameters is provided in Table 1.

3. EXPERIMENTAL RESULTS

In **Figure 2**, the measured and predicted stress-strain response is shown for the three in-situ compression tests performed parallel to RD. Note that the serrations in the flow curves are due to the load relaxation, which occurs during the time of 20 minutes per measurement, required to collect neutrons. The unloads to near zero stress reveal a slight hysteresis. As is typical of many materials, the flow stress decreases as the temperature is increased. Additionally, the strain hardening rate decreases from a slope of around 3 GPa at room temperature to a low slope of just under 1 GPa at 150 °C. At 100 °C, an intermediate hardening rate of about 1.8 GPa is observed,

so the transition appears to be gradual over this temperature range. The polycrystal plasticity model is able to describe the decrease in aggregate flow stress (based on the temperature dependences of individual single-crystal deformation mechanisms, as determined by Knezevic et al [14]). In addition, the decrease in the aggregate hardening behavior is well described by empirical fitting of the linear hardening rates of the two hard deformation modes denoted roof and chimney, whereas the hardening behavior of the softer modes appears to be athermal, in the present rate and temperature regime.

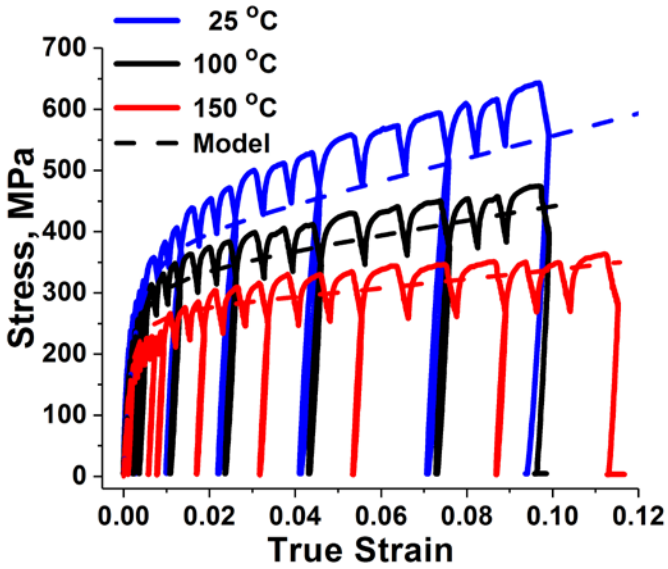

Figure 2. Stress-strain response from compressive loading along the RD at three different temperatures on SMARTS.

Figure 3 shows the measured and predicted internal strain evolutions for cases which account for and neglect thermal residual stresses. It is seen that the internal strain predictions change greatly with the inclusion of thermal residual stresses even as the temperatures increase. At all temperatures, the grains with an (002) pole parallel to the loading axis have the highest level of internal strain. Thus, they appear to be the strongest (most resistant to plastic deformation, since they accumulate the most elastic deformation). More interestingly, although the (200) oriented grains are stronger at room temperature than the (040) grains, as temperature increases, the (040) grains begin to appear stronger than the (200) grains. This observation is explained by a combination of Schmid factor analysis and the thermal residual stress state. Based on Schmid factors, the (040) grains are well oriented for $\{\bar{1}30\}$ twinning during compression, while the (200)

grains are well suited for chimney or wall slip. The slip modes soften with temperature, while the resistance to the twinning mode does not (it behaves athermally). Single crystal studies of α-uranium have revealed that the resistance to $\{\bar{1}30\}$ twinning decreases only slightly with temperature in comparison to the slip modes [6].

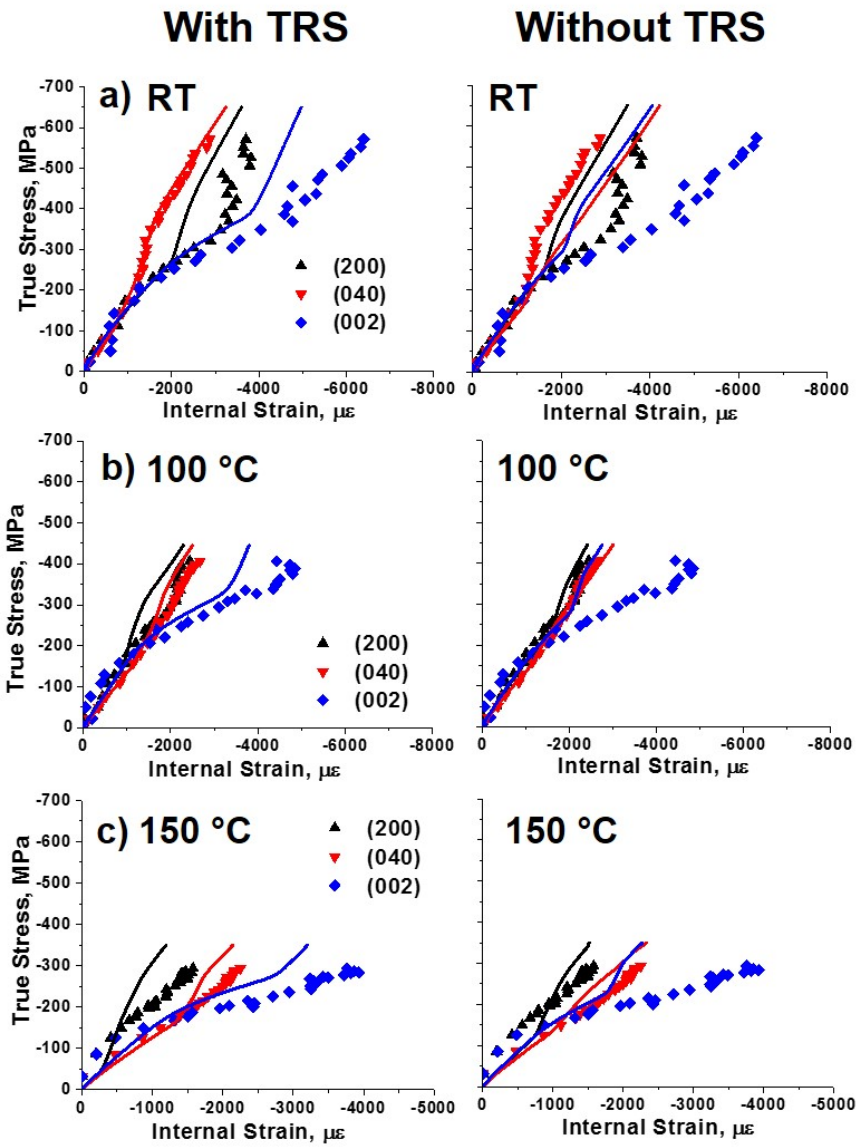

Figure 3 Comparison of the predicted (lines) and measured (symbols) internal strain evolutions for the (a) room temperature, (b) 100 °C, and (c) 150 °C experiments that account for thermal residual stresses (left) and neglect thermal residual stresses (right)

The thermal stresses experienced by the grains with (020) or (040) poles parallel to the loading direction are compressive, since the thermal expansion along the (020) is far lower than the surrounding polycrystal. This is especially true along the normal direction of the plate, the direction along which the plate has the largest thermal expansion coefficient. As the sample is heated, the thermal stresses are relaxed, so the residual strains along the (020) direction become less compressive, and those along the (200) and (002) become less tensile. Since the sample is being compressed, the reduction of compressive stress due to thermal mismatch makes the (040) oriented grains appear stronger as temperature is increased. **Figure 4** shows a comparison of the measured and predicted strains in the (040) oriented grains. It is seen that including the effects of thermal residual stress enables the model to qualitatively predict the observed behavior without introducing hard to rationalize behavior, such as increasing the resistance to twinning.

Large shifts in normalized peak intensity indicate the activity of deformation twinning, since the intensity is proportional to the volume of material in the diffraction condition, and twinning results in a certain volume fraction of the corresponding parent material adopting a new (twin) crystallographic orientation. **Figure 5** shows a plot of the relative diffraction peak intensities during deformation. (Normalized or relative means normalized by the initial intensity, in this context.) The (040) grains are well oriented for $\{\bar{1}30\}$ twinning during compression, so the drastic decrease in peak intensity beginning (at about 300 MPa at room temperature) can be correlated with the onset of $\{\bar{1}30\}$ twinning in this set of grains. The {131} and {021} oriented grains are not well suited for this twin mode, but rather the less prevalent {172} twin mode. A simultaneous rise in intensity occurs in the {110} peak along with a drop in {131} and {021} intensities, at around 400 MPa at room temperature. At room temperature and 100 °C, the {110} orientation only gains volume fraction during loading. However, at 150 °C, the {110} diffraction peak first loses intensity then starts to gain intensity. The {110} grains are well orientated to twin by the $\{\bar{1}30\}$ mode, but at the lower temperatures it does not activate prior to the onset of twinning in other grains, such as those which contribute to {131} and {021} peaks, which appear to contribute to the increasing intensity of the {110} diffraction peak.

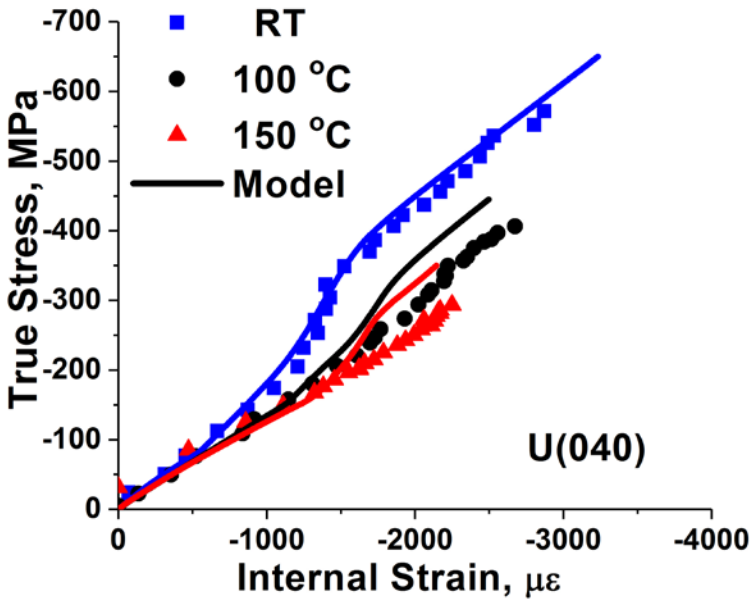

Figure 4 Comparison of the predicted (lines) and measured (symbols) internal strain evolutions along the (040) direction at RT (blue) , 100 °C (black) , and 150 °C (red) experiments that account for thermal residual stresses.

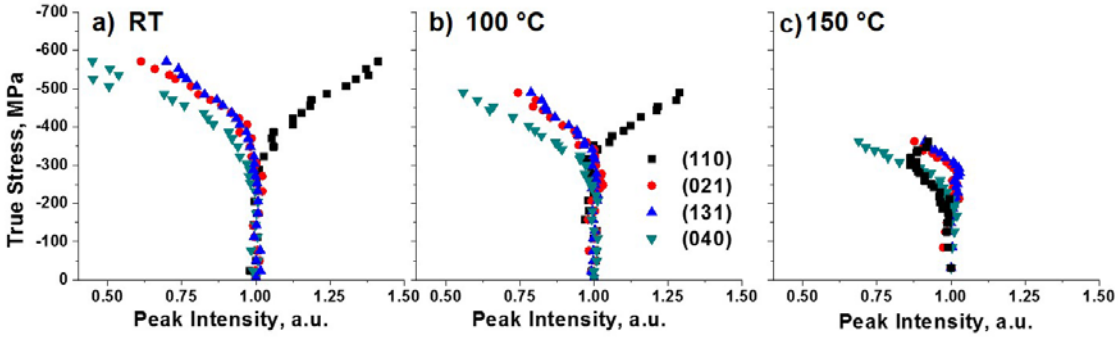

Figure 5. Plot of the normalized peak intensity along the loading direction indicating shifts in orientation due to deformation twinning at (a) RT, (b) 100 °C and (c) 150 °C.

4. MODELING AND DISCUSSION

Determination of the specific prior (parent) orientation of the new volume fraction is not possible with the current type of diffraction experiment. However, it is possible to identify which twin modes *could* or *could not* explain the observed intensity evolutions in **Figure 5** by comparing the angles between the diffracting plane normal vectors and the characteristic twinning rotation

axis[†]. This rotation axis corresponds to a shared (invariant) axis within the twin and parent. Therefore, this axis must make the same angle with the scattering vector, $\boldsymbol{\Delta k}$, in order for the observed shifting of diffraction intensity to be explained by the twinning variant in question. **Figure 6** presents a schematic illustration of the relationship between the scattering geometry (Laue equations demand $\boldsymbol{\Delta k}||\boldsymbol{n}(hkl)$ where $\boldsymbol{n}(hkl)$ is normal to the plane (hkl)), and the elements of twinning, $\boldsymbol{\eta}_1$ and $\boldsymbol{x}_2$. In short, if the angle between the diffraction vector and the rotation vector is constant between the candidate twin and parent, then activation of that twin mode *could* explain the observed shift in intensity from one diffraction peak to the other.

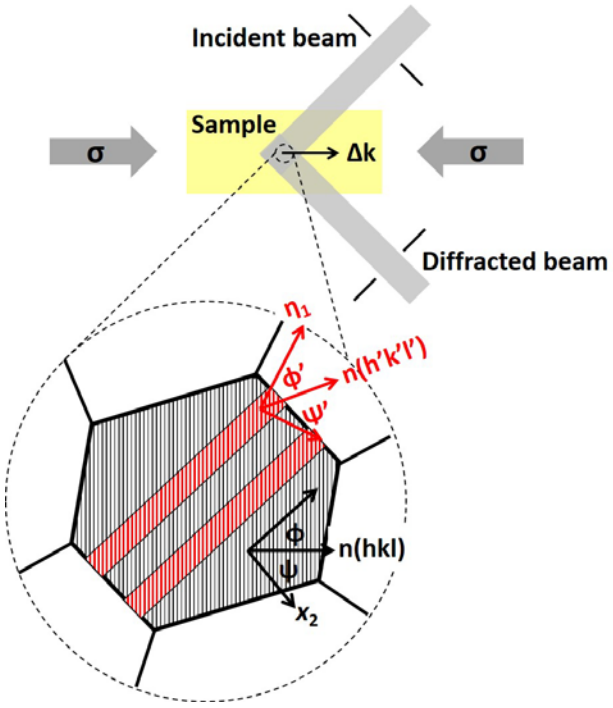

Figure 6. Schematic illustration of the diffraction geometry and relationship to twinning elements.

For the rather unusual case of type II twins, such as {172} twins in α-uranium, the angle,ϕ', between the candidate diffraction plane normal $\boldsymbol{n}(h'k'l')$ within the twin and the twin shear direction $\boldsymbol{\eta}_1$ must be equal to the angle, ϕ, from the shear direction to the plane normal $\boldsymbol{n}(hkl)$ of interest within the parent. For the more common twins of the first kind, the angle, ψ', between the candidate plane normal $\boldsymbol{n}(h'k'l')$ within the twin and the twin plane normal $\boldsymbol{x}_2$ must be equal to

[†] The symmetry of type I twins is equivalent to a 180° rotation about the pole of the twinning plane, K_1, denoted as $\boldsymbol{x}_2$ in Figure 6, whereas type II twins are characterized by a 180° rotation about the twin shear direction, commonly denoted $\boldsymbol{\eta}_1$. Compound twins exhibit both symmetries.

the angle, ψ, with the plane normal $\boldsymbol{n}(hkl)$ within the parent. For compound twins, such as the {130} twins in α-uranium, both conditions must be met. Thus, one can eliminate possibilities for which the angles between the invariant axes are not common between the two in question *hkl*'s.

Table 2 lists the angles between the relevant diffraction plane normal vectors and the candidate twinning rotation axes. In order to determine these angles, the indices of the relevant directions were converted to Cartesian coordinates [U V W] = [*ua vb wc*] and then normalized. Similarly, the Miller indices of the planes were converted as follows (H K L) = (*h/a k/b l/c*) and then normalized. Then, the angle between the two was computed as the inverse cosine of the dot product between the two (which is tantamount to using the reciprocal lattice concept). It is seen that there are similar angles between the variants of $\langle 3\bar{1}2\rangle$ vectors (the $\boldsymbol{\eta}_1$ directions for {172} twins) and (110) and (021) diffraction peaks (44° vs. 45° which could both diffract into a given detector). Similar observations can be made for the angles 69° and 65° to the (110) and (131) planes, respectively. Therefore, {172} twinning could explain the observed intensity evolutions. On the other hand, since the $\{\bar{1}30\}$ twin is a compound twin, both the shear direction and the twin plane normal must make similar angles with the diffraction vectors. As such, even though the (110) pole for the second variant makes has a similar angle with the $\langle 3\bar{1}0\rangle$ direction as the (021), the twin plane poles do not coincide. As such, the $\{\bar{1}30\}$ mode would not connect any of the observed intensity shifts between these diffraction peaks.

Table 2. Angles between the diffraction vectors and the twinning rotation vectors (all variants) for the two twin modes

Peak	$\langle 3\bar{1}2\rangle$				$\langle 3\bar{1}0\rangle$		{130}	
	1	2	3	4	1	2	1	2
(110)	44	69	69	44	8	60	30	70
(131)	31	78	78	65	28	90	18	70
(021)	45	90	45	90	61	61	45	45

The {040} oriented grains are known to twin by the $\{\bar{1}30\}$ mode based upon EBSD measurements [8]. Therefore, the decrease in {040} peak intensity is due to $\{\bar{1}30\}$ twinning.

However, there is not a corresponding increase in the intensity of any of the other peaks monitored, since the resulting twins would not be in a diffraction condition. In contrast, the onset of {172} twinning, which is considered a secondary mode [8], in the grains closely oriented to {131} or {021} diffracting conditions, could cause an increase in the {110} or {112} intensity. The simultaneous drop and rise in intensity of these respective peaks, at all three temperatures, suggests that the {131} and {021} oriented grains drop intensity due to {172} twinning, and the corresponding twins contribute to the increase in {110} or {112} diffraction peak intensity. The grains which contribute to the {110} peak represent roughly 1% of the volume fraction, while the {131} and {021} peaks represent 5% and 3%, respectively. As such, twinning in the initially {110} oriented grains would not necessarily be seen in such a plot. The shifts in internal residual stresses are believed to cause the onset of twinning in {110} grains prior before twinning in {131} grains at the higher temperature, while at room temperature, the twinning in the {131} grains occur first. Again, ex-situ EBSD studies have revealed the dominance of $\{\bar{1}30\}$ twinning [8]. It is noted that because the study was conducted on unloaded samples, it is possible that detwinning occurred during the unload.

EPSC modeling allows for the estimation of relative contributions of the different deformation modes, **Figure 7**, with residual stress included (a-c) and residual stress neglected (d-f) for deformation at RT, 100, and 150 °C, respectively. To compute relative activity, the shear strain for each mode is divided by total shear in each grain and then volume averaged over the entire polycrystal. In all of the simulations, the wall mode activates very early in the deformation and accommodates nearly all of the plastic deformation, but there are only small levels of plastic strain at this point. Therefore, it is emphasized that a high relative activity does not necessarily mean a large absolute level of strain is accommodated. Nevertheless, this observation does highlight the fact that the wall mode is the softest mode, which activates early.

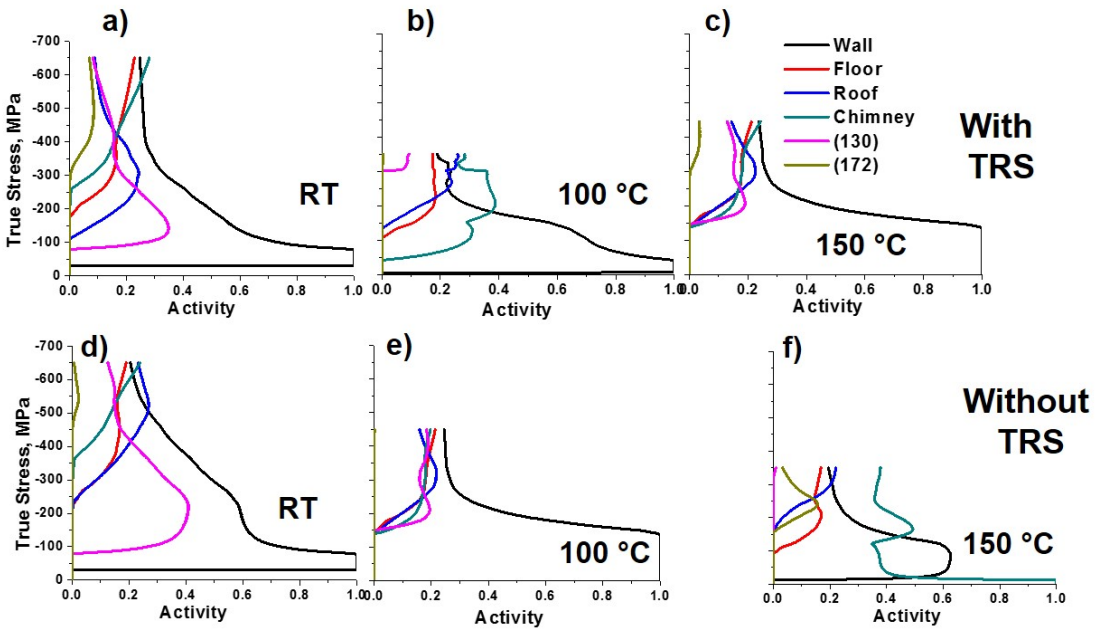

Figure 7. Plot of the relative slip and twin mode activity during deformation at (a) RT, (b) 100 °C and (c) 150 °C when including thermal residual stresses, and (d) RT, (e) 100 °C and (f) 150 °C when neglecting thermal residual stress.

When analyzed together with the internal strain evolution presented in **Figure 3**, the relative activity plots do help identify the cause of inflections in the internal strain evolution within different grain sets. In all the simulations, yield in the {040} oriented grains coincides with the onset of the $\{\bar{1}30\}$ twin mode. The plots also show a decrease in twin activity and increase in slip activity as temperature increases, which is expected, given the thermally activated nature of slip and near athermal character of twinning in the temperature range of interest [6]. The model predicts a shift in the order of activation of the slip modes, as the chimney mode softens much more than the roof mode at these mildly elevated temperatures [14]. At room temperature, the chimney mode activates after the roof mode, despite having a lower CRSS. Once again, this is due to the presence of thermal residual stresses (**Figure 7** a-c). In all the simulations, the roof and floor modes activate simultaneously. This is required for macroscopic flow, but activation of the roof mode corresponds to inflection in the internal strain evolution of the {002} grains, which is not seen until higher stress levels in the experiment. This shortcoming is likely a result of uncertainty in the thermal residual stress predictions. Notably, the current model [11] permits relaxation by crystallographic slip alone, whereas, there is evidence in favor of more isotropic diffusion-controlled flow

mechanisms (such as dislocation climb and grain boundary sliding) as primary modes of internal stress relaxation [20].

The crystallographic texture of each specimen was measured after the heating, mechanical deformation and subsequent cooling for the sample tested at 150 °C and this can be compared with the texture evolution at room temperature, **Figure 8.** The current EPSC model allows for prediction of the texture evolution due to twinning during deformation. **Figure 8** shows the measured and predicted pole figures for samples. At room temperature, RD compression results in large twinning volume fractions at room temperature, as seen previously [8]. This results in significant texture evolution during deformation (**Figure 7** c-d). This strong change in texture was both observed experimentally and predicted by the EPSC simulation. In fact, the texture evolution is somewhat over-predicted, which suggests that the model over estimates the activity of the $\{\bar{1}30\}$ twinning mode, as all the (010) intensity is lost along the rolling direction during room temperature deformation. At higher temperatures, the measured and simulated texture evolves much less. As the temperature increases, the slip modes become softer, and deformation twinning contributes much less to the overall plastic deformation.

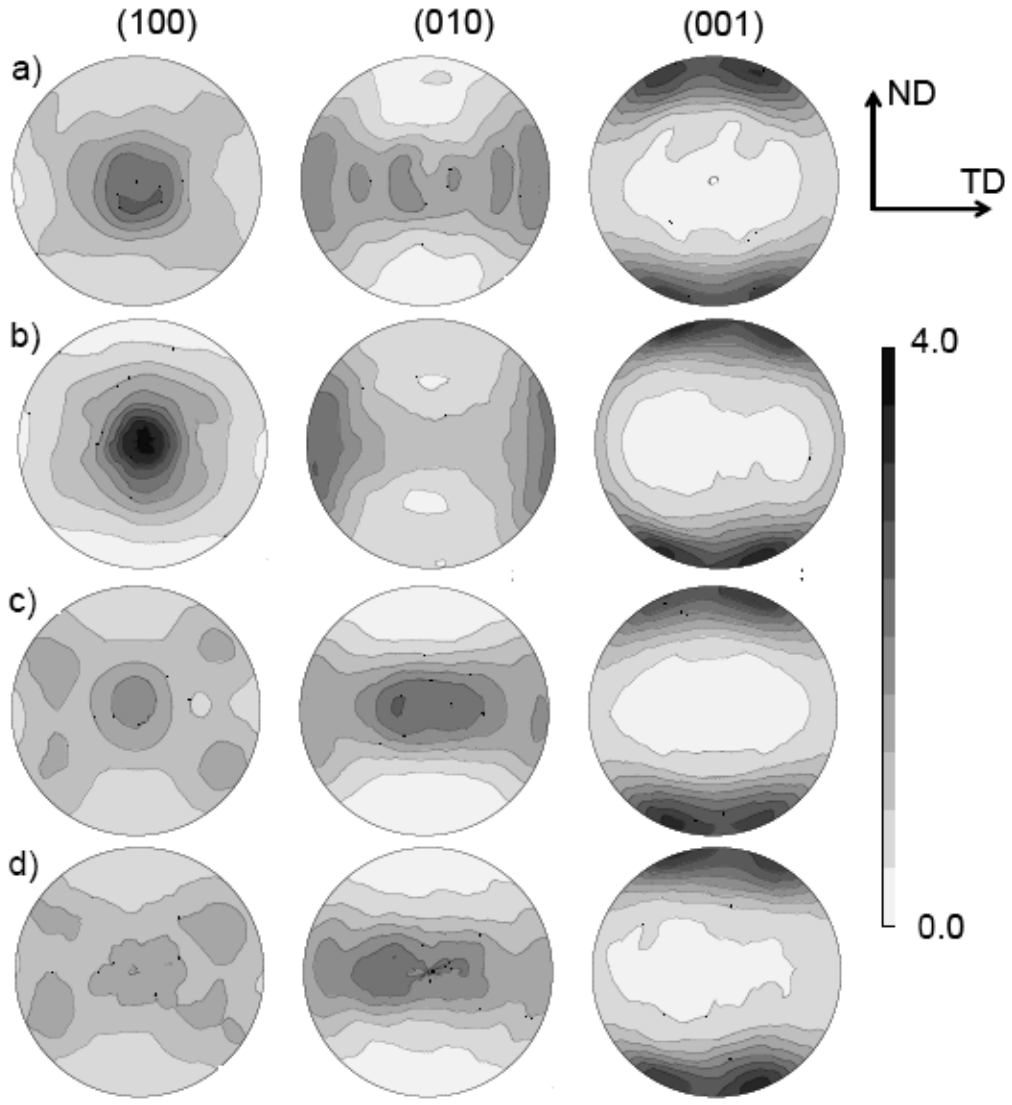

Figure 8. Post deformation textures: (a) measured after 9.5 % strain at room temperature, (b) predicted after 12% strain at room temperature, (c) measured after 11% strain 150 °C, and (d) predicted after 12 % strain at 150 °C.

CONCLUSIONS

In-situ neutron diffraction data analyzed with the help of polycrystalline thermo-elastic-plastic modeling leads to the following conclusions regarding the fundamental behavior of depleted, orthorhombic α-uranium:

- Both the yield strength and strain hardening rate decrease with increasing temperature.

- Modeling the internal strain evolution measured through diffraction requires accounting for thermal residual stress. By implication, determining the relative strengths of the deformation modes through polycrystalline plasticity modeling requires proper accounting of the thermal stresses.
- The EPSC code predicted the rank order of the internal strains, and macroscopic flow curves by employing a previously generated model for thermal residual stresses, by employing temperature sensitivities of the slip mechanisms, which were previously determined using a VPSC model.
- The internal stress development during heating from room temperature cause an apparent increase in strength in grains well oriented for twinning, especially the grains with (040) poles parallel to the loading direction.
- The {110} peaks gain intensity during loading at room temperature and 100 °C, but first decrease in intensity before later increasing at 150 °C. Again, the internal stress state induces this apparent variation in strength of the $\{\bar{1}30\}$ twinning mode.
- The decrease in {021} and {131} peak intensities and simultaneous increase in {110} and {112} intensities suggest the activation of the secondary {172} twinning mode within the {021} and {131} grains.
- Due to an increase in slip activity and decrease in twinning, the texture evolves to a lesser extent at higher temperatures when compressing along the rolling direction, as evidenced by both the measured and EPSC simulated pole figures.

ACKNOWLEDGEMENTS

The authors would like to thank D. W. Brown of Los Alamos National Laboratory for his assistance in conducting the neutron experiments. Funding for this research was provided by the Y-12 National Security Complex under the Plant Directed Research and Development program. This work of authorship and those incorporated herein were prepared by Consolidated Nuclear Security, LLC (CNS) as accounts of work sponsored by an agency of the United States Government under Contract DE NA 0001942. Neither the United States Government nor any agency thereof, nor CNS, nor any of their employees, makes any warranty, express or implied, or assumes any legal liability or responsibility to any non-governmental recipient hereof for the accuracy, completeness, use made, or usefulness of any information, apparatus, product, or process

REFERENCES

[1] E S Fisher and H J McSkimin, "Adiabatic Elastic Moduli of Single Crystal Alpha-Uranium," *Journal of Applied Physics,* vol. 29, no. 10, pp. 1473-1484, 1958.

[2] L T Lloyd, "Thermal Expansion of alpha-uranium single crystals," *Journal of Nuclear Materials*, vol. 3, no. 1, pp. 67-71, 1961.

[3] J Korn, "An Investigation of the Cones of Zero Expansion and Thermal Coefficients for Single Crystal of alpha-Uranium," *Journal of Nuclear Materials*, vol. 71, no. 2, pp. 320-326, 1978.

[4] R W Cahn, "Plastic Deformation of alpha-Uranium: Twinning and Slip," *Acta Metallurgica*, vol. 1, no. 1, pp. 49-70, 1953.

[5] M H Yoo, "Slip modes of alpha uranium," *Journal of Nuclear Materials*, vol. 26, no. 3, pp. 307-318, 1968.

[6] J S Daniel, B Lesage, and P Lacombe, "The influence of temperature on slip and twinning in uranium," *Acta Metallurgica*, vol. 19, no. 2, pp. 163-173, 1971.

[7] W S Blackburn, "The effect of internal stresses due to irradiation growth and thermal cycling on the creep of uranium, in the cases of both elastic and plastic behaviour," *Journal of Nuclear Energy. Parts A/B. Reactor Science and Technology,* vol. 14, no. 1, pp. 107-116, 1961.

[8] R J McCabe, L Capolungo, P E Marshall, C M Cady , and C N Tome, "Deformation of wrought uranium: Experiments and modeling," *Acta Materialia,* vol. 58, no. 16, pp. 5447-5459, 2010.

[9] A G Crocker, "The crystallography of deformation twinning in alpha-uranium," *Journal of Nuclear Materials*, vol. 16, no. 3, pp. 306-326, 1965.

[10] R D Field, R J McCabe, D J Alexander, and D F Teter, "Deformation twinning and twinning related fracture in coarse-grained alpha-uranium," *Journal of Nuclear Materials*, vol. 392, no. 1, pp. 105-113, 2009.

[11] C A Calhoun et al., "Thermal Residual Strains in Depleted alpha-U," *Scripta Materialia*, vol. 69, no. 8, pp. 566-569, 2013.

[12] P A Turner and C N Tome, "A study of residual stresses in Zircaloy-2 with rod texture}," *Acta metallurgica et Materialia*, vol. 42, no. 12, pp. 4143-4153, 1994.

[13] D W Brown et al., "Temperature and direction dependence of internal strain and texture evolution during deformation of uranium," *Materials Science and Engineering: A*, vol. 512, no. 1, pp. 67-75, 2009.

[14] M Knezevic et al., "Modeling mechanical response and texture evolution of alpha-uranium as a function of strain rate and temperature using polycrystal plasticity," *International Journal of Plasticity*, vol. 43, pp. 70-84, 2012.

[15] C A Calhoun, E Garlea, R P Mulay, T A Sisneros, and S R Agnew, "Investigation of the effect of thermal residual stresses on deformation of Î±-uranium through neutron diffraction measurements and crystal plasticity modeling," *Acta Materialia*, vol. 85, pp. 168-179, 2015.

[16] H R Wenk, L Lutterotti, and S Vogel, "Texture analysis with the new HIPPO TOF diffractometer," *Nuclear Instruments and Methods in Physics Research Section A: Accelerators, Spectrometers, Detectors and Associated Equipment*, vol. 515, no. 3, pp. 575-588, 2003.

[17] MA M Bourke, D C Dunand, and E Ustundag, "SMARTS--a spectrometer for strain measurement in engineering materials," *Applied Physics A*, vol. 74, pp. 1707-1709, 2002.

[18] B Clausen, C N Tome, D W Brown, and S R Agnew, "Reorientation and stress relaxation due to twinning: modeling and experimental characterization for Mg," *Acta Materialia*, vol. 56, no. 11, pp. 2456-2468, 2008.

[19] H Wang, P D Wu, C N Tome, and J Wang, "A constitutive model of twinning and detwinning for hexagonal close packed polycrystals," *Materials Science and Engineering A*, vol. 555, pp. 93-98, 2012.

[20] C A Calhoun, *Thermomechanical Response of Polycrystalline alpha-Uranium*, Dissertation, Ed. Charlottesville, VA, USA: University of Virginia, 2016.